ADVANCED ENERGY MATERIALS
www.advenergymat.de

All-Solid-State Lithium-Ion Microbatteries Using Silicon Nanofilm Anodes: High Performance and Memory Effect

Frédéric Le Cras, Brigitte Pecquenard,* Vincent Dubois, Viet-Phong Phan, and Delphine Guy-Bouyssou*

All-solid-state thin film lithium batteries are promising devices to power the next generations of autonomous microsystems. Nevertheless, some industrial constraints such as the resistance to reflow soldering (260 °C) and to short-circuiting necessitate the replacement of the lithium anode. In this study, a 2 V lithium-ion system based on amorphous silicon nanofilm anodes (50–200 nm thick), a LiPON electrolyte, and a new lithiated titanium oxysulfide cathode $Li_{1.2}TiO_{0.5}S_{2.1}$ is prepared by sputtering. The determination of the electrochemical behavior of each active material and of whole systems with different configurations allows the highlighting of the particular behavior of the Li_xSi electrode and the understanding of its consequences on the performance of Li-ion cells. Lithium-ion microbatteries processed with industrial tools and embedded in microelectronic packages exhibit particularly high cycle life (–0.006% cycle^{-1}), ultrafast charge (80% capacity in 1 min), and tolerate both short-circuiting and reflow soldering. Moreover, the perfect stability of the system allows the assignment of some modifications of the voltage curve and a slow and reversible capacity fade occurring in specific conditions, to the formation of $Li_{15}Si_4$ and to the expression of a "memory effect." These new findings will help to optimize the design of future Li-ion systems using nanosized silicon anodes.

1. Introduction

The significant growth of both the number and the kinds of portable electronic systems, generally battery-powered, has triggered the race for the development of high-performance microprocessors and systems-on-a-chip (SoCs) using low power consumption integrated circuits. As a consequence, the energy supply of such optimized components can also be ensured today by miniaturized power sources such as microbatteries (whose capacities range from 1 to 100 µAh). All-solid-state lithium microbatteries have the advantage of being manufactured by vacuum deposition processes, also widely used in the microelectronics industry,[1,2] and not to contain a liquid electrolyte, this being beneficial to safety. The association of microelectronic components and microbatteries will possibly give birth to new products within three main domains—back-up power "UPS (Uninterruptible power Supply)-like" for dynamic random access memory (DRAM) or real-time clocks (RTC), embedded energy and autonomous devices. Nevertheless, these new applications require that the microbattery has sufficient thermal stability to tolerate the reflow soldering to attach the component to a circuit board. When using lead-free solders, i.e., Sn—Ag—Cu eutectics, the microbattery must sustain temperatures higher than 230 °C.[3] Lithium microbatteries are not tolerant to such high temperatures as they contain a lithium metal anode that melts at 181 °C. Thus, two possible solutions exist: (i) the use of a "lithium-free" configuration in which all the lithium is initially contained in the discharged cathode,[4] the first charge leading to the plating of metallic lithium on the negative current collector and (ii) the use of a real lithium-ion cell, with a negative electrode material able to reversibly react with lithium at low voltage, and melting at a temperature higher than 260 °C. In both cases, the microbattery is theoretically tolerant to short-circuiting which is also a great advantage for manufacture and use.

As for "lithium-free" stacks, it was clearly evidenced that the electroplating of lithium at the surface of the bare current collector (negative electrode) is generally not uniform and depends on the current density applied during the charge.[5] Indeed, low current densities lead to a limited amount of nucleation sites for metallic lithium, hence favoring the growth of large packs of lithium, and finally leading to mechanical damage in the cell and a fast capacity fade.[4,6]

Only a few complete all-solid-state lithium-ion thin film cells were reported in the literature. Negative electrode materials

Dr. F. Le Cras
Université Grenoble Alpes
CEA LETI, Minatec Campus
Grenoble 38054, France
E-mail: frederic.lecras@cea.fr
Prof. B. Pecquenard, Dr. V. Dubois, Dr. V.-P. Phan
CNRS, Université de Bordeaux
ICMCB, UPR 9048
Pessac 33608, France
E-mail: brigitte.pecquenard@icmcb.cnrs.fr
Dr. V. Dubois, Dr. V.-P. Phan, Dr. D. Guy-Bouyssou
ST Microelectronics
Tours 37071, France

DOI: 10.1002/aenm.201501061

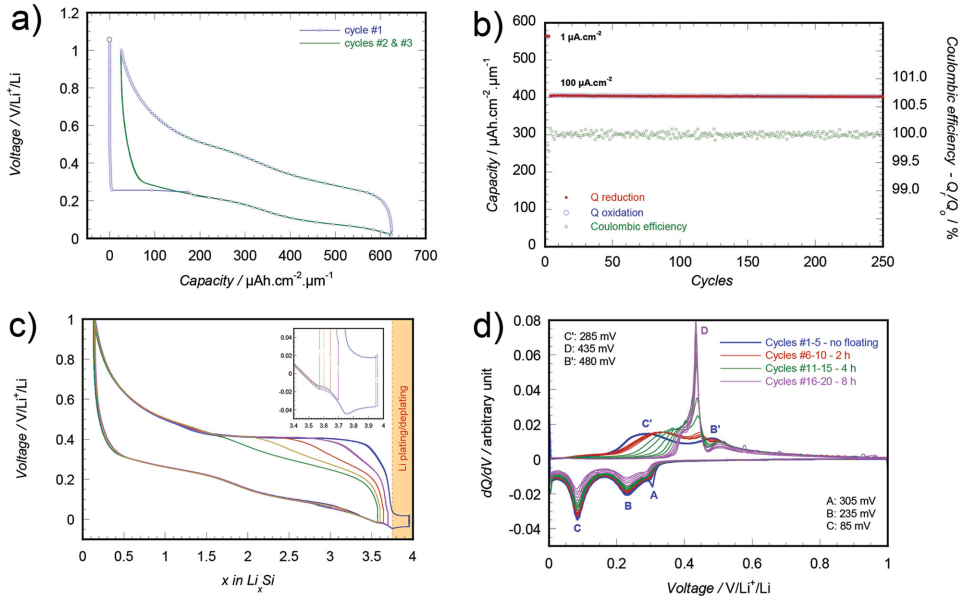

Figure 1. Electrochemical features of Si(100 nm)/LiPON/Li microbatteries: a) Voltage curves for the three first discharge/charge cycles at constant current (53 µA cm^{-2}, 0.02–1 V/Li^+/Li), b) evolution of the capacity and the coulombic efficiency (1–100 µA cm^{-2}, 0.05–1 V/Li^+/Li), c) influence of the low cut-off voltage on the shape of the voltage curve (formation of $Li_{15}Si_4$, 10 µA cm^{-2}), and d) evolution of the derivative capacity $\partial Q/\partial V$ for increasing floating durations at 0 V/Li^+/Li applied at the end of galvanostatic cycles (10 µA cm^{-2}), showing the progressive increase of the amount of $Li_{15}Si_4$ revealed by peak D.

associated with $LiCoO_2$ and LiPON were $SiSn_{0.87}O_{1.20}N_{1.72}$ "LiSiTON",[7] tin nitride,[8,9] and tin oxide,[10] which all lead to an important capacity loss (30%–50%) during the first cycle. Indeed, these materials react with lithium in two main steps involving: (i) a conversion reaction $xLi^+ + xe^- + MX \rightarrow M + Li_xX$ (M: metal, X: N, P, O, S, Se, F) and (ii) an electrochemical alloying reaction $yLi^+ + ye^- + M + Li_xX \rightarrow Li_yM + Li_xX$. The reversibility of the first reaction step inside a given voltage window greatly depends on the thickness (or the particle size) of the electrode material, and the nature of X and M.[11]

Other systems such as V_2O_5/LiPON/$LiMn_2O_4$,[12,13] and Al/LiPON/$Li_xCo_yMn_3O_8$,[14] were not able to provide a stabilized capacity.

In this paper, we report for the first time on the manufacture and the characterization of all-solid-state lithium-ion cells containing a lithiated titanium oxysulfide positive electrode and based on a thin film silicon negative electrode. Indeed, in order to avoid lithium being trapped during the first cycle as Li_2O or Li_3N in the negative electrode, pure elements forming alloys with lithium are preferred candidates. Among them, most were ruled out here for different reasons: (i) Ga, In, Sn, and Pb due to their low melting point, (ii) Cd, Hg, and Tl due to their toxicity, (iii) Pt, Pd, and Au due to their cost, (iv) alkaline earth metals due to their reactivity, and finally (v) Sb and Bi due to a too high delithiation voltage. Finally, among the remaining candidates (Al, Si, Zn, Ge, and Ag), silicon has already proved to be a high-performance electrode in all-solid-state Li/LiPON/Si thin film cells despite the huge volume variations of the Li_xSi material occurring during the charge/discharge cycles.[15] At room temperature, the maximum amount of lithium that can be inserted by electrochemical alloying corresponds to the formation of the $Li_{15}Si_4$ compound,[16] and leads to the high theoretical volumetric capacity of 835 µAh cm^{-2} $µm^{-1}$.

To be compatible with the low voltage supply required for low-consumption microsystems, a titanium oxysulfide (TiOS) thin film positive electrode was envisaged to obtain an expected operating voltage comprised between 1.5 and 2 V. The TiOS amorphous material is able to deliver a high volumetric capacity (90–100 µAh cm^{-2} $µm^{-1}$) compared to $LiCoO_2$ (64 µAh cm^{-2} $µm^{-1}$) and does not require an additional annealing step.[1,17] In this work, a new lithiated TiOS positive electrode was synthesized by sputtering of an $LiTiS_2$ target and was then associated with the silicon negative electrode to form an Li-ion cell.

2. Results and Discussion

2.1. Nanosized Silicon Thin Film Electrodes in All-Solid-State Lithium Batteries

Silicon thin film electrodes prepared by radio-frequency sputtering with no intentional heating of the substrate are amorphous and quite dense. The film thickness of 100 nm was chosen to obtain a surface capacity in the range 60–80 µAh cm^{-2}, close to the surface capacity for 1 µm thick positive electrodes ($LiCoO_2$, $LiMn_2O_4$, TiOS, etc.). In addition, this thickness is advantageously smaller than the critical size (150 nm) above which the fracture of silicon is likely to occur during lithiation/delithiation cycles.[18] The electrochemical behavior of silicon thin films was studied in all-solid-state Si/LiPON/Li "half-cells." As shown in **Figure 1**a, the first reduction starts with a small irreversible reaction at ≈0.3 V/Li^+/Li which involves only 2% of the total capacity. This latter is specific to all-solid-state cells and

is very likely related to the reduction of SiO_xN_y species formed at the electrode–electrolyte interface during the deposition of LiPON on the top of the silicon electrode. Then, the reduction proceeds in two main steps centered at 0.23 and 0.08 V/Li^+/Li, each one involving approximately half of the total capacity. It has to be noticed that this last step, close to 0 V/Li^+/Li, is often not completed nor even initiated during the operation of most conventional cells using (nano)silicon electrodes and liquid electrolyte cells,[19] due to a too significant polarization (ohmic drop, sum of concentration and activation overpotentials). Consequently, a prolonged operation of Li_xSi electrodes in the Li-rich region was rarely achieved in the literature.

As for our all-solid-state thin film batteries, the theoretical volumetric capacity of 834 µAh cm^{-2} $µm^{-1}$ was never reached in normal cycling conditions using constant currents. The flatness of the voltage curve shape at low potential makes the actual discharge capacity very sensitive to the discharge cut-off voltage and to the reduction overpotential. Then, the practical capacity when using a lower cut-off voltage ranging from 0.02 to 0.05 V/Li^+/Li and a current density ranging from 1 to 100 µA cm^{-2}, varies between 400 and 600 µAh cm^{-2} $µm^{-1}$.

The subsequent oxidation allows removing 98% of the lithium from the Li_xSi electrode during two main steps located at ≈0.28 and 0.48 V/Li^+/Li. The voltage hysteresis between reduction and oxidation is about 200–230 mV and is quite constant over all the composition range. This electrochemical behavior is consistent with the presence of only amorphous or short-range ordered Li_xSi compounds. Subsequently, the cycle life of the Li/LiPON/Si all-solid-state cells is almost perfect as the capacity loss is only −0.003% $cycle^{-1}$ (Figure 1b), despite the large volume changes of the Li_xSi electrode.

As first shown by Obrovac and Christensen,[16] the lithiation of the silicon electrode at room temperature can be completed up to the $Li_{15}Si_4$ composition, inducing the crystallization of the corresponding material. In their liquid electrolyte cells, the tiny reduction step triggering the formation of $Li_{15}Si_4$ was found to occur at 50 mV/Li^+/Li, while the main electrochemical feature of the formation of this crystallized end member is the modification of the shape of the voltage curve during the subsequent oxidation, with the presence of a marked plateau at around 0.44 V/Li^+/Li. In all-solid-state thin film batteries, the formation of this compound was not so easy. As shown in Figure 1c, the voltage at which the final reduction step occurs in our solid electrolyte cells is located below 0 V/Li^+/Li (–15 to –45 mV), even when using a very low current density, due to the sum of reaction overpotentials on both electrodes (two-electrode cell). This final step involves only 5% of the total lithium content (from $Li_{\approx 3.6}Si$ to $Li_{3.75}Si$), but has a large influence on the shape of the voltage curve during the subsequent oxidation. Besides, it demonstrates that the formation of crystallized $Li_{15}Si_4$ from amorphous Li_xSi is not a congruent process.[20] During galvanostatic cycling, the only means to get a complete lithiation of the silicon electrode was either to carry on with the reduction until metallic lithium starts to plate on the Li_xSi electrode (Figure 1c), or to add a floating period at the end of the discharge. Considering the latter point, as shown on the derivative curve (Figure 1d), more than 2 h of floating at 0 V/Li^+/Li are necessary to initiate the formation of some crystalline $Li_{15}Si_4$ phase in the Li_xSi thin film. Nevertheless, whatever the cycling conditions, once the formation of some $Li_{15}Si_4$ has occurred at the end of a given discharge, its formation seems easier and amplified during the subsequent ones. This behavior is clearly highlighted by a continuous increase of the intensity of peak D at 0.44 V/Li^+/Li, when a 4 h floating is applied. These observations are consistent with the in situ X-ray diffraction study achieved on silicon nanowires by Misra et al.,[21] that also evidenced a kinetic limitation of the formation of $Li_{15}Si_4$ and a more widespread crystallization after a second cycle. This suggests that a progressive modification of the (micro)structure of the silicon thin film occurs after each full lithiation/full delithiation cycle, making the formation of $Li_{15}Si_4$ easier. The formation of a mesoporous silicon network, once the electrode is delithiated,[22] is probably at the origin of the enhancement of the $Li_{15}Si_4$ formation kinetics, as it could progressively lead to an optimized arrangement of silicon atoms that minimizes Si diffusion path lengths throughout the film during the subsequent alloying reaction.

In addition to the features of the Si thin film electrochemical behavior detailed above, another particular evolution of the voltage curve leading to a reversible capacity fade ("memory effect") was highlighted in a previous study, for thin films cycled in liquid electrolyte in specific conditions.[23] As a reminder, it was evidenced that a prolonged cycling in the Li-rich region (i.e., below 0.44 V/Li^+/Li) induces a progressive increase of deinsertion voltage above this cut-off limit, hence a capacity loss in the part of the voltage curve lying below this value. Subsequently, the full capacity and the initial shape of the voltage curve can be recovered after a full delithiation that reveals the presence of a new electrochemical step at 0.51 V/Li^+/Li (i.e., distinct from the lithium deinsertion step from $Li_{15}Si_4$) (see Figure S1, Supporting Information).

To summarize, to ensure a perfectly stable electrochemical behavior of amorphous silicon thin film electrodes, it is mandatory to avoid the formation of the $Li_{15}Si_4$ compound or the possible ordering of Li-rich alloys; this can be achieved by maintaining the lower cut-off voltage above 0.05 V/Li^+/Li and regularly carrying out a full delithiation.

2.2. Lithiated Titanium Oxysulfide Thin Film Electrodes

As for TiOS thin films, LiTiOS electrodes deposited with no intentional heating of the substrate are amorphous. The structure of the film is dense, with a density close to 2.7 g cm^{-3} (crystalline $LiTiS_2$: 3 g cm^{-3}) and a very smooth surface. Combined chemical analyses by Rutherford backscattering (RBS) (**Figure 2**a), inductively coupled plasma optical emission spectrometer (ICP-OES), and electron probe microanalysis (EPMA) lead to the following composition $Li_{1.2}TiO_{0.5}S_{2.1}$, and confirm the incorporation of a small amount of oxygen into the film. Auger depth-profile analyses (Figure 2b) demonstrate the chemical homogeneity of the film across the whole thickness. Additional XPS analyses clearly show that the oxygen incorporation in the film induced a full reoxidation of titanium into Ti^{4+} and, contrary to TiOS, did not lead to the formation of S_2^{2-} species.[24,25] All these elements are consistent with a positive electrode material formula $Li_{1.2}Ti^{IV}O_{0.5}S^{II}_{2.1}$.

A full electrochemical delithiation of $Li_{1.2}TiO_{0.5}S_{2.1}$ electrode corresponding to a capacity of 64 µAh cm^{-2} $µm^{-1}$ was achieved in all-solid-state half-cells (**Figure 3**a); as Ti^{4+} cannot be involved

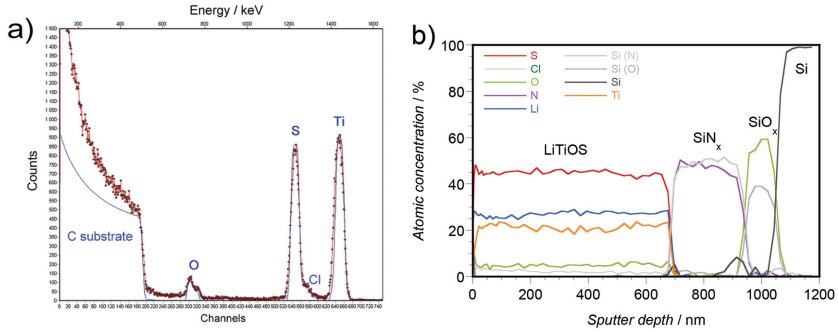

Figure 2. Elemental analyses of lithiated titanium oxysulfide thin films obtained by sputtering of an $LiTiS_2$ target: a) RBS spectrum of a 100 nm thick film and b) Auger electron spectroscopy depth-profiling analysis of a thin film deposited on a passivated silicon wafer. Note that chlorine traces were initially present in the TiS_2 precursor, probably produced by sulfidation of $TiCl_4$.

in this oxidation process, it means that the sulfide species are actually oxidized during charge up to 2.9 $V/Li^+/Li$, forming S_2^{2-} disulfide anions. The subsequent lithiation and delithiation curves, showing no capacity loss, demonstrate the perfect reversibility of the electrochemical processes. Actually, when cycled in the 3.2–1.5 V voltage window versus a lithium anode, extra lithium can be inserted in the $Li_{1.2}TiO_{0.5}S_{2.1}$ material below ≈2 $V/Li^+/Li$. Below this limit, titanium is partly reduced. The successive reductions of disulfide species, then of Ti^{4+} at lower potential, were also observed during the lithiation of the non-lithiated starting material $TiO_{0.6}S_{2.3}$.[25] Then, the formation of a mixed valence compound having a higher electronic conductivity is probably the reason for the far lower voltage hysteresis observed between the charge and the discharge in the region of Ti activity (ΔE = 100 mV) than in the region of S activity (ΔE = 300 mV). Finally, slow sweep voltammetry experiments (Figure 3b) highlight the presence of a single broad step, both for the reduction and the oxidation of sulfur, centered, respectively, around 2.24 and 2.64 $V/Li^+/Li$.

As shown in Figure 3c, the increase of the current density from 2 to 130 μA cm^{-2} (i.e., *C*-rates from *C*/50 to 2*C*) induces only a slight capacity decrease, mainly due to an increase of the polarization near the end of charge. Besides, the capacity retention is found to be excellent during extended cycling with a capacity fading lower than –0.01% $cycle^{-1}$ and a mean coulombic efficiency close to 100%. Finally, $Li_{1.2}TiO_{0.5}S_{2.1}$ is confirmed as a new interesting lithiated positive material for moderate-to-low voltage thin film lithium and lithium-ion microbatteries. Moreover, as its synthesis does not require any thermal treatment, it is well-adapted to thermally sensitive substrates such as flexible polymers foils.

2.3. Si/LiPON/$Li_{1.2}TiO_{0.5}S_{2.1}$ Lithium-Ion Microbatteries

2.3.1. Influence of the Capacity Balancing between Positive and Negative Electrodes

All-solid-state LiTiOS/LiPON/Si lithium-ion cells were manufactured on three silicon wafers using for each a different

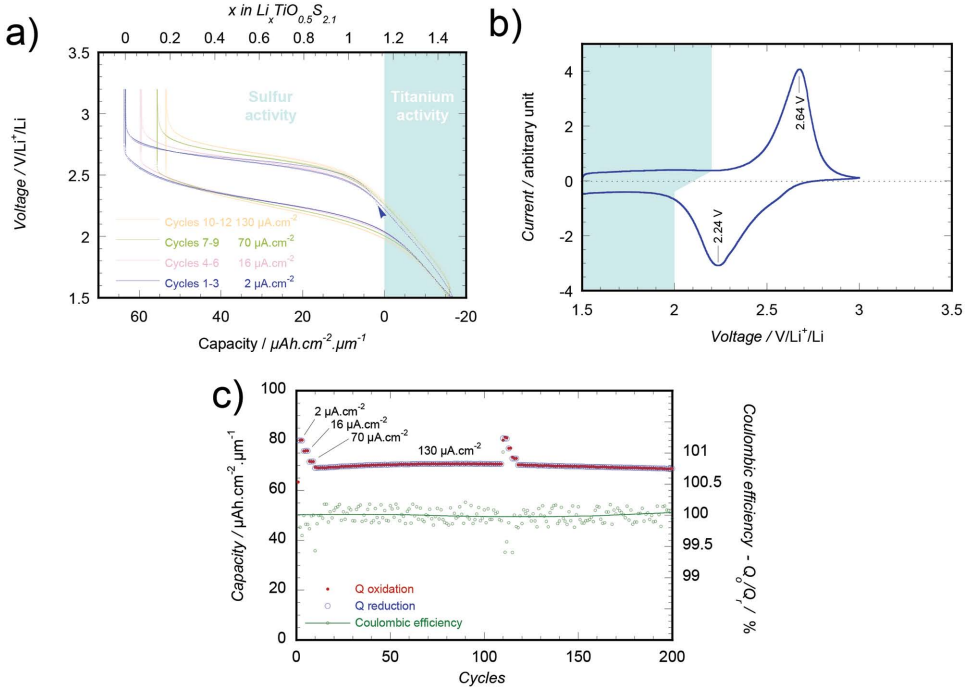

Figure 3. Electrochemical features of $Li_{1.2}TiO_{0.5}S_{2.1}$(1070 nm)/LiPON/Li microbatteries: a) Voltage curves measured at various constant current densities, b) voltammogram (sweep rate 5 μV s^{-1}), and c) evolution of the capacity as a function of the current density (1.5–3.2 $V/Li^+/Li$) and cycle life at 130 μA cm^{-2} (*C*/1.5 rate).

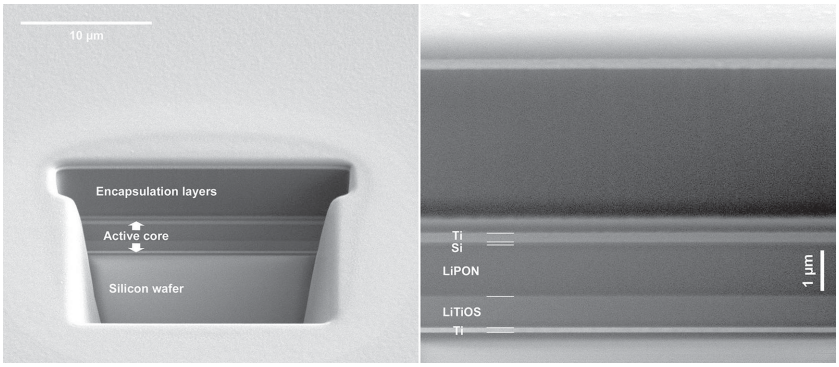

Figure 4. FIB/SEM cross section of a thin film encapsulated lithium-ion microbattery comprising the $Li_{1.2}TiO_{0.5}S_{2.1}$/LiPON/Si active layers and titanium current collectors.

capacity balancing between the positive and the negative electrodes, in order to evaluate its influence on the voltage curve of the Li-ion cell and the irreversible capacity. This was achieved by using different thicknesses for the silicon electrode (80, 120, and 180 nm), while keeping the thickness of the positive electrode nearly constant around 1.1 µm. The surface capacity available for the positive is then close to 70 µAh cm^{-2}, and the one of the silicon negative electrode is equal to, respectively, 50, 70, and 110 µAh cm^{-2}. A scanning electron microscopy (SEM)/FIB cross-section view of a complete stack is provided in **Figure 4**. As common features for the three types of cells, the expected capacity from the positive electrode is obtained during the first charge on reaching 2.9 V and a similar irreversible capacity (2 µAh cm^{-2}) is observed at the end of the first discharge (**Figure 5**a). The latter is very close to the one measured for Li/LiPON/Si half-cells and is undoubtedly related to irreversible processes occurring at the LiPON/Si interface where "SiO_xN_y" species are formed during the realization of the microbattery.

As the design of such all-solid-state thin film Li-ion batteries does not allow the use of a reference electrode, the most convenient way to follow the course of Li insertion in (and extraction from) electrodes is provided by the voltage derivative of the capacity ($\partial Q/\partial V$) calculated from the galvanostatic experiments. As the insertion/deinsertion of lithium in the lithiated titanium oxysulfide generates a single broad peak (Figure 3b), the different marked steps on $\partial Q/\partial V$ plots for Li-ion cells (Figure 5b–d) result from the electrochemical reactions occurring at the Li_xSi negative electrode. When a 180 nm thick Si film is used as negative electrode, only slightly more than half of the Si capacity is used, hence it is expected that only the first insertion step in Si (peak B on Figure 1d) and a small part of the second one (peak C) are involved during the operation. The presence of a main peak with a shoulder at higher potential on the $\partial Q/\partial V$ plot (Figure 5b) is then fully consistent. When using a cell with a 120 nm thick silicon electrode, hence balanced electrode capacities ("balanced cell"), the two main Li insertion/deinsertion steps (peaks B/B′ and C/C′) now appear clearly on the $\partial Q/\partial V$ plot (Figure 5c) both during the charge and the discharge of the Li-ion cell. Finally, when the capacity of the positive electrode exceeds the one of the silicon electrode (80 nm thick), the extra peak that comes out at higher potential (≈2.8 V) at the end of charge and its counterpart at the beginning of the discharge are both a clear evidence of lithium plating/deplating on the negative electrode at high state-of-charge (Figure 5d). Similar to Li/LiPON/Si cells (Figure 2c,d), lithium plating on the Li_xSi thin film is found to be concomitant with the formation of the crystallized $Li_{15}Si_4$ compound. In these Si deficient lithium-ion cells, the latter is revealed by a marked modification of the derivative plot during the discharge and the appearance of an intense peak located at ≈1.95 V (peak D), which corresponds to the delithiation of $Li_{15}Si_4$ that actually occurs at 0.44 V/Li^+/Li. In addition, a small irreversible step is systematically observed at 2.16 V for all cells at the beginning of the first charge (peak A); it corresponds to

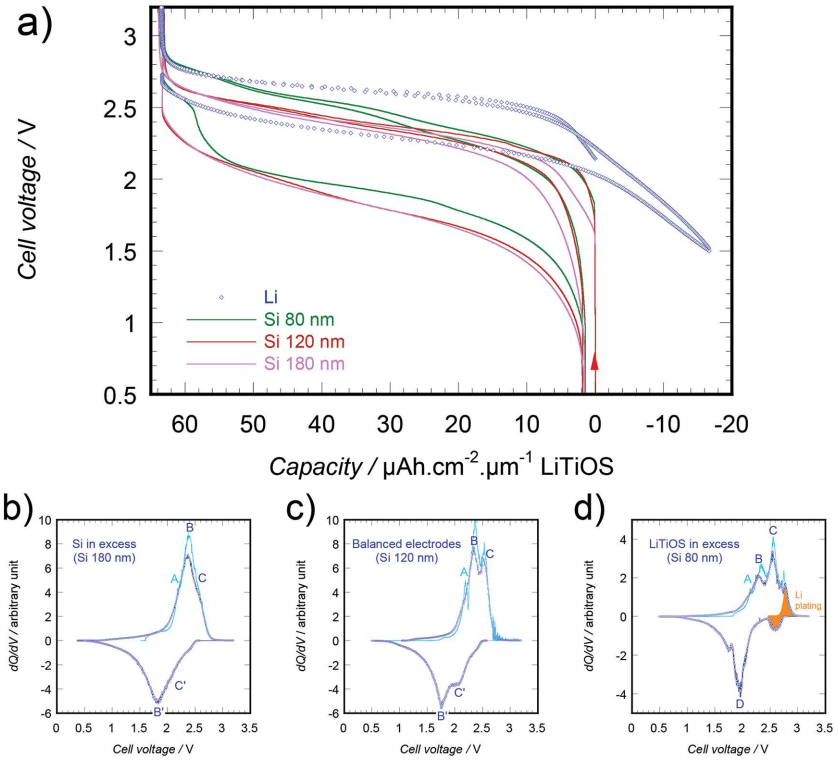

Figure 5. a) Voltage curves of the first 1.5 cycle of lithium-ion cells based on different Si/LiTiOS ratios. The voltage curve of an Li/LiTiOS cell is given for comparison. The positive electrode thickness is kept constant to 1.1 µm. Voltage derivative of the capacity $\partial Q/\partial V$ obtained for a negative electrode having, respectively, b) a higher capacity (Si 180 nm), c) the same capacity (Si 120 nm), and d) a lower capacity (Si 80 nm) than the positive electrode. The first charge appears in light blue.

the "depassivation" reaction observed at 0.3 V/Li^+/Li during the first reduction of the silicon electrode (peak A on Figure 1a).

Finally, the electrochemical response of the three different full LiTiOS/LiPON/Si Li-ion cells is in perfect accordance with the expected behavior deduced from the virtual assembly of Si and LiTiOS half-cells characterized previously. A preliminary assessment of the cycle life of the three configurations of Li-ion microbatteries was carried out. The best stability of the capacity during prolonged cycling at ≈2*C* rate (130 µAh cm^{-2}) was obtained with the balanced assembly (Si 120 nm) and the worst with the assembly using the thinner silicon electrode (Si 80 nm) that leads to lithium plating (see Figure S2, Supporting Information). More than 1200 cycles were achieved with LiTiOS/LiPON/(Si 120 nm) cells, leading to a mean capacity fading of about –0.015% $cycle^{-1}$.

The critical difference between a virtual assembly of half-cells and the final lithium-ion assembly is the presence of a metallic lithium electrode. Indeed, as the capacity of the lithium electrode is always several times higher than the capacity of the working electrode (Si or LiTiOS), the lithium contained in the negative electrode is able to compensate continuously for a loss of lithium previously located in the working electrode. Moreover, lithium can also act as a getter and consequently can prevent water or oxygen from corroding the other constituents of the microbattery, especially the working electrode. As a consequence, the capacity of the thin film Li-ion cells and its stability (vs cycles, vs time) are far more sensitive to small amounts of water or oxygen reaching the active part of the cell than that of lithium metal cells. As an example, the permeation through the packaging of 0.04 µg H_2O can lead directly to 1% capacity loss in these 25 mm^2 cells, by oxidation (delithiation) of the Li_xSi negative electrode. At this stage, it cannot be excluded that the quality of the encapsulation layers surrounding the active part of these lab-scale lithium-ion microbatteries is a main factor governing their cycle life and their calendar life.

2.3.2. Electrochemical Behavior of Balanced Lithium-Ion Microbatteries Produced and Packaged Using Industrial Equipment

A new series of LiTiOS/LiPON/Si lithium-ion microbatteries having a smaller footprint (8.7 mm^2 active area) was produced

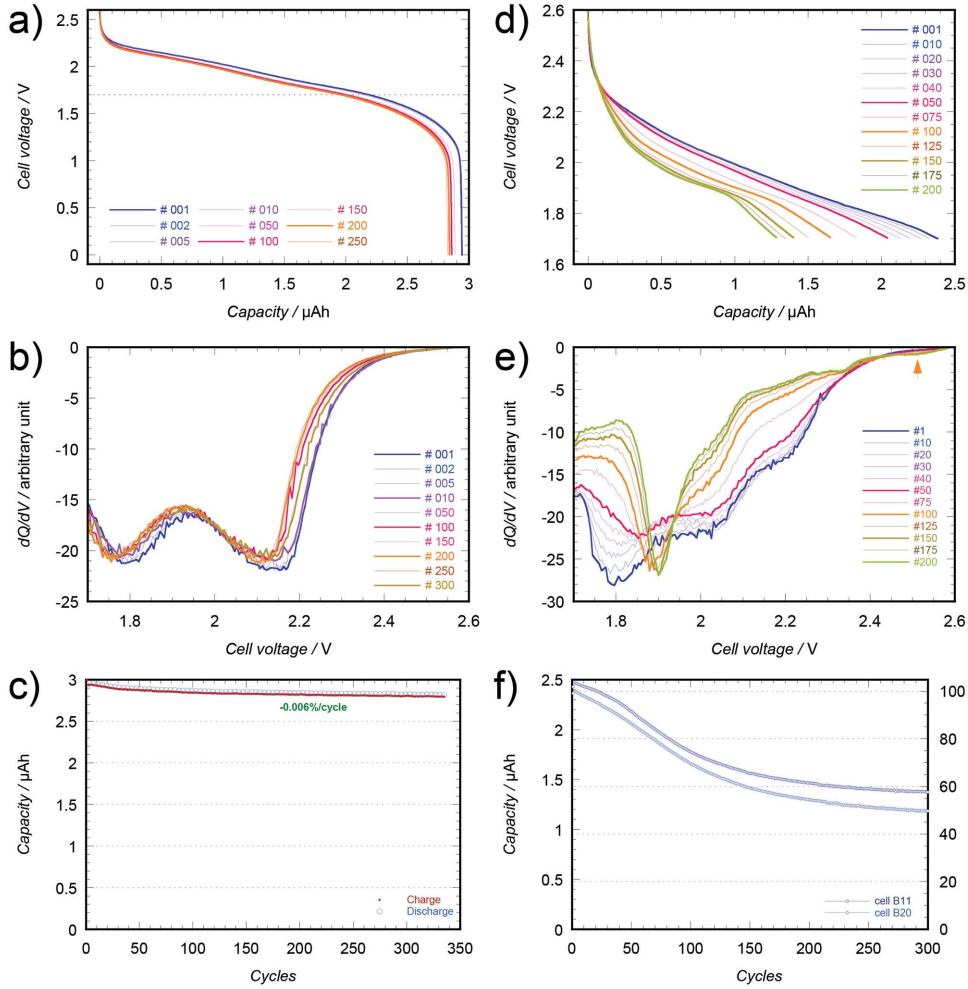

Figure 6. Electrochemical behavior of 8.7 mm^2 Li-ion microbatteries embedded in LGA packages. a,d) Discharge curves, b,e) voltage derivative of the capacity $\partial Q/\partial V$, and c,f) capacity retention of cells discharged at constant current, respectively, to 0 and 1.7 V, before the thermal treatment at 260 °C (solder-reflow).

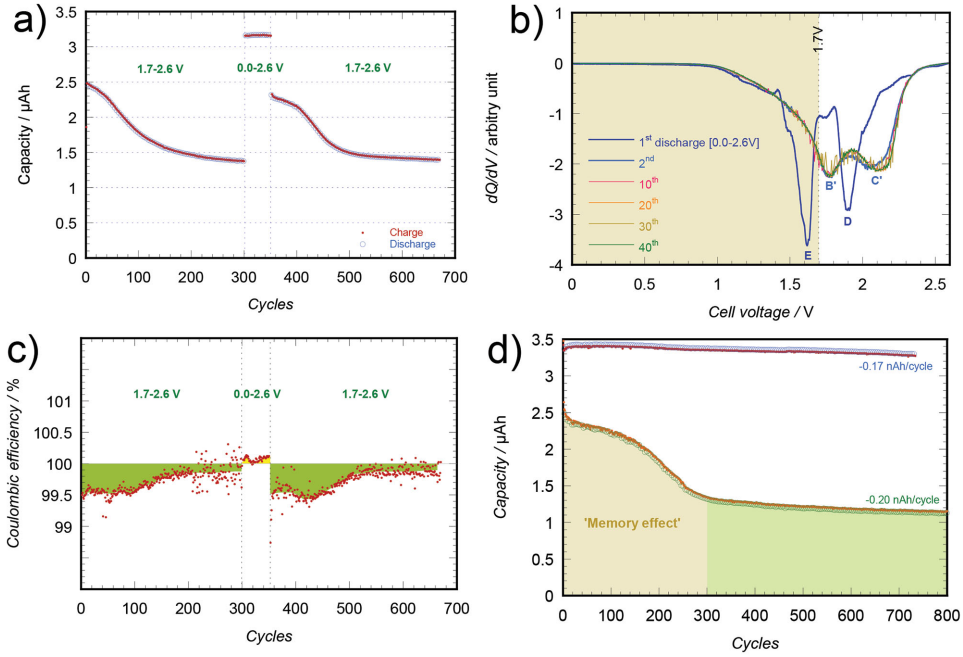

Figure 7. a) Evolution of the capacity of a microbattery during three successive sequences with a low cut-off voltage of either 1.7 or 0 V, b) ∂Q/∂V derivative curves for the first discharge to 0 V and the subsequent ones, following 300 cycles in the 1.7–2.6 V, b) evolution of the coulombic efficiency of the same microbattery, and d) capacity retention of two cells cycled continuously either in the 0–2.6 or the 1.7–2.6 range.

on 8 in. diameter silicon wafers. These microbatteries were processed in industrial facilities as conventional electronic components and were encapsulated in land grid array (LGA) packages (5×5 mm^2) in order to check the performance of the energy storage component in more realistic conditions. LGA packages, which are widely used in the microelectronics industry, are manufactured by injection molding of a blend of epoxy resin (10%) and fused silica as a filler (90%) around the electronic component, completed by a curing step (typically 175 °C during 6 h) to achieve the cross-linking of the resin. As a consequence, the mold compound is fully dried and acts as an additional barrier to moisture.

The electrochemical behavior of these packaged microbatteries (65 nm thick silicon electrodes and balanced configuration) was studied prior to and after three heat treatments reproducing the thermal profile of a lead-free solder reflow. The specific cycling conditions applied at room temperature were: (i) charge at constant voltage (2.6 V) until the current decreases to 100 nA and (ii) discharge at constant current (5 µA, i.e., 60 µA cm^{-2}) with two different values of cut-off voltage, 0 V to assess the tolerance to short-circuiting or 1.7 V for a normal operation.

Short-Circuit Tolerance Tests: Lithium-ion cells cycled between 2.6 and 0 V, prior to the solder-reflow treatment, exhibit a voltage profile (**Figure 6**a) similar to the one obtained with the previous series of balanced cells. In particular, the shape of the derivative curve (Figure 6b), highlighting the two main lithium deinsertion steps from silicon and the absence of lithium deplating, is fully consistent with the operation of a balanced cell (Figure 5c). As for the evolution during prolonged cycling, the voltage profile appears very stable during the 350 cycles and an excellent capacity retention is obtained with a capacity fade not exceeding –0.006% cycle^{-1} (Figure 6c). These results allow us to conclude that: (i) the industrial processing of microbatteries after their deposition on silicon wafers did not damage the cells, (ii) embedding the cells in an LGA package enhanced their cycle/calendar life, and (iii) there is no detrimental effect of discharging the cell to 0 V. The latter point is actually one of the main specific requirements from OEM (Original Equipment Manufacturer) end users, with the compatibility with the solder-reflow process.

Memory Effect in Lithium-Ion Cells: Afterward, other fresh microbatteries were cycled with the same procedure, except that the cycles were performed between 1.7 and 2.6 V. During the charge at constant voltage (Figure S3, Supporting Information), 70% and 80% of the capacity were delivered, respectively, in 30 s and 1 min. This ultrafast charging performance is even better than the one measured for the lithiation of silicon thin film electrodes (70 nm thick) in liquid electrolyte half-cells.[26] But surprisingly, a slow but marked modification of the voltage curve (Figure 6d) and its derivative (Figure 6e) was then observed during prolonged cycling in these conditions, accompanied by a significant decrease of the delivered capacity (Figure 6f). After 200 cycles, the derivative curve of the discharge exhibits a sharp peak at ≈1.9 V and a tiny step at 2.5 V (see also Figure S4, Supporting Information). The clear similarity with the behavior of an Si-deficient cell (Figure 5d) highlights the presence of a growing amount of $Li_{15}Si_4$ and plated lithium on the negative electrode at the end of each charge. Then, when resuming cycles with discharges down to 0 V, after 300 cycles carried out in the previous conditions, it was very astonishing to observe that the cell actually behaved perfectly. Indeed, a full and stable capacity (**Figure 7**a), as well as the conventional shape of the derivative curve (Figure 7b) were observed, respectively, from the first and the second discharge to 0 V.

The derivative curve of the first full discharge (Figure 7b) and the evolution of the coulombic efficiency (Figure 7c) actually give the key to understanding the progressive capacity loss that occurred when cycling in the 1.7–2.6 V window and the progressive emergence of the $Li_{15}Si_4$ phase. Indeed, the first full discharge at 0 V shows that the lithium "lost" during the previous 300 cycles can actually be deinserted from the negative electrode during a new important electrochemical step (peak E) located at 1.6 V (i.e., just below the previous cut-off voltage). The position of this peak relative to the position of the C′, D, and B′ peaks corresponding to identified delithiation steps in the silicon electrode (see Li/LiPON/Si cell in Figure 1d) allows the estimation of its position around 0.55 V/Li^+/Li. Besides, the evolution of the coulombic efficiency showed that, during each cycle carried out in the 1.7–2.6 window, the amount of lithium inserted in the silicon electrode was higher than the amount of lithium extracted during the following discharge of the cell. It means that lithium progressively accumulated in the negative electrode due to a modification of the voltage curve of the Li_xSi electrode. Such a phenomenon has already been reported and described for silicon thin film electrodes charged/discharged in liquid electrolyte cells in given voltage windows.[24] It was called "memory effect" due to its similarity to the capacity decay observed when nickel–cadmium cells are not fully discharged. In silicon electrodes, this so-called memory effect develops slowly when a high lithium content is maintained in the Li_xSi electrode, and is erased each time a delithiation of the silicon electrode is performed above 0.6 V/Li^+/Li. In the present case, it means that these balanced Si/LiPON/LiTiOS cells should be discharged below 1.45 V to overcome this effect or to recover their initial behavior.

As for the $Li_{15}Si_4$ phase and metallic lithium formed at the end of the charge, they are probably located at Si electrode–electrolyte interface due to lithium diffusion limitations when the high lithium flow is generated at the beginning of the charge at constant voltage. Although absent during the first cycles performed in the 1.7–2.6 V window, lithium plating and the formation of $Li_{15}Si_4$ is certainly progressively favored as the lithium content remaining in the whole silicon electrode progressively increases due to the memory effect. Once a stationary behavior was reached in the 1.7–2.6 V window (i.e., after ≈300 cycles), the capacity fade stabilizes at a value (–0.2 nAh $cycle^{-1}$ or –0.006% $cycle^{-1}$) close to the one measured for cells tested in the 0–2.6 V window (–0.17 nAh $cycle^{-1}$), indicating that the formation of $Li_{15}Si_4$ or the plating of small amounts of metallic lithium on the negative electrode have no marked detrimental effects on the cycle life of the microbattery (Figure 7d).

Solder-Reflow Tolerance: A similar electrochemical study was carried out on Si/LiPON/LiTiOS cells after three successive thermal treatments at 260 °C (solder-reflow). The capacity, the cycle life, the voltage profile of the lithium cells (**Figure 8**a,b), and the emergence of the memory effect remained finally unchanged after this operation (Figure S5, Supporting Information).

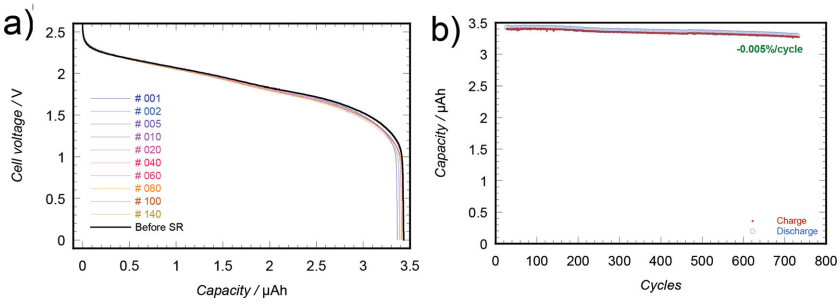

Figure 8. a) Discharge curves and b) capacity retention in the 0–2.6 V voltage window of a microbattery that underwent three successive thermal treatments (solder-reflow).

3. Conclusion

For the first time, all-solid-state Li-ion thin film batteries manufactured at the industrial scale have given the unique opportunity to characterize the performance and the behavior of nanometer-sized (50–200 nm thick) silicon thin film electrodes in real Li-ion cells and during extended periods of time. The perfect stability (–0.006% $cycle^{-1}$) and reproducibility of Si/LiPON/LiTiOS cells allowed the highlighting or the confirmation of the occurrence of specific phenomena developing slowly in the silicon electrode and their consequences on the behavior of silicon-based lithium-ion cells. A reversible capacity fade reported as memory effect was found likely to appear, depending on the electrode capacity balancing and the operating voltage window. This will have to be taken into account in particular for designing future high-energy density lithium-ion cells based on nanosized silicon negative electrodes.

Finally, silicon nano-film anodes allowed the achievement of ultrafast charging, short-circuit, and solder-reflow tolerant all-solid-state lithium-ion batteries, therefore adapted for various microelectronic applications.

4. Experimental Section

Manufacture of All-Solid-State Thin Film Batteries: Microbatteries were manufactured using sputtering and evaporation deposition of thin films

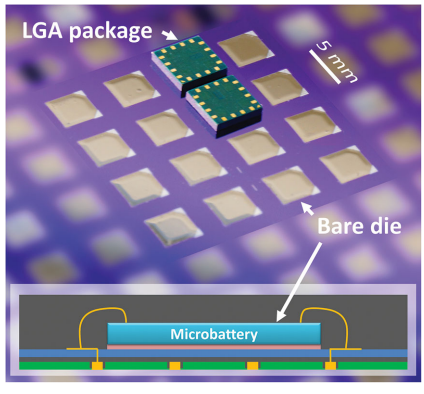

Figure 9. Photograph showing thin film encapsulated lithium-ion microbatteries (bare dies) deposited on an 8 in. diameter silicon wafer and the same embedded in a 5 × 5 mm^2 LGA package at the end of the manufacturing process; sketch of a bonded microbattery embedded in an LGA package.

Table 1. Summary of deposition conditions for the different thin films.

Material	Thickness [μm]	Film manufacturing process
Silicon wafer	500	NA
Barrier layers	0.240	Thermal oxidation, low-pressure CVD
W	0.250	Sputtering W target
		DC mode: $P = 2.8$ W cm^{-2}, $P_{tot} = 0.9$ Pa, Ar 100%
		Deposition rate = 25 nm min^{-1}
$Li_xTiO_yS_z$	≈1	Sputtering $LiTiS_2$ target
		RF mode: $P = 1.27$ W cm^{-2}, $P_{tot} = 0.5$ Pa, Ar 100%
		Deposition rate = 8 nm min^{-1}
LiPON	1.400	Sputtering Li_3PO_4 target
		RF mode: $P = 2$ W cm^{-2}, $P_{tot} = 2$ Pa, N_2 100%
		Deposition rate = 5 nm min^{-1}
Si	0.080–0.160	Sputtering Si target
		DC mode: $P = 0.34$ W cm^{-2}, $P_{tot} = 0.5$ Pa, Ar 100%
		Deposition rate = 13 nm min^{-1}
Li	≈3	Thermal evaporation
		Deposition rate = 60 nm min^{-1}
Ti	0.250	Sputtering Ti target
		DC mode: $P = 2.5$ W cm^{-2}, $P_{tot} = 0.5$ Pa, Ar 100%

on a 4 in. silicon wafer substrate covered by barrier layers. Cells having various electrode areas equal to, respectively, 8.7, 18.7, 25, or 96 mm^2 were prepared by patterning each film level either by photolithography or shadow masking. The encapsulation was achieved by polymer/metal thin films multilayers, and then reinforced by a glass cap for cycling during long periods of time. A complete integration in 5 × 5 mm^2 LGA packages was achieved for a specific series of 8.7 mm^2 Li-ion cells produced with industrial tools on 8 in. silicon wafers (**Figure 9**).

Three types of battery stacks were used for this study: half-cells associating either an $Li_xTiO_yS_z$ or a silicon working electrode with a lithium metal counter electrode, and finally $Li_xTiO_yS_z$ and Si in an Li-ion assembly. Thin films were successively deposited in the following order: a metal current collector, the positive electrode, an LiPON vitreous electrolyte, the negative electrode, then possibly a second metal current collector.

The first series of microbatteries were manufactured in a lab-scale deposition tool (Plassys) directly connected to a glove box. The $LiTiS_2$ sputtering target (2 in. diameter) was prepared from a crystallized $LiTiS_2$ powder, obtained by chemical lithiation of TiS_2 (Aldrich) with *n*-butyl lithium in excess (1.6 M in hexane, Aldrich) as reported elsewhere,[27] and then cold pressed at 60 MPa. The sputtering target for the preparation of the electrolyte was obtained by cold pressing and sintering of pure Li_3PO_4 powder (Aldrich). Its ionic conductivity, 2×10^{-6} S cm^{-1} at 20 °C, was measured by impedance spectroscopy analysis. Finally, the silicon target (99.999%) was directly purchased from Neyco. The substrate was water-cooled during all the deposition process. The deposition parameters of each active layer are summarized in **Table 1**.

Then, this process was finally up-scaled for the deposition of 8.7 mm^2 microbatteries on 8 in. silicon wafers, in an industrial deposition tool using 12 in. targets (Endura cluster, Applied Materials).

Characterization of Thin Films: The composition of LiTiOS thin films was determined from RBS measurements (CENBG, Gradignan), EPMA, and ICP analyses. Electron microprobe analysis (Cameca SX100) and RBS were used to determine Ti, O, and S contents. RBS experiments were performed at a backscattering angle of 150° using an incident beam of $^4He^+$ ions with energy of 2 MeV. For that purpose, sample thin films with a thickness of 100 nm were deposited onto polished glassy carbon substrates. Spectra were then processed using the SIMNRA software.[28] Finally, the Li content was measured by using an ICP-OES (Varian 720ES) and the 460.289 nm Li wavelength emission line. Sample solutions were prepared by dissolving LiTiOS thin films deposited on a glass substrate in 10 mL of diluted HCl.

The homogeneity of the LiTiOS film composition was checked by Auger spectroscopy depth profiling (VG MICROLAB 310F apparatus). Thin film thickness was measured with a Dektak 6M profilometer.

Microbattery cross sections were visualized using a high-resolution field effect scanning electron microscope (FE-SEM) coupled with a precise focused ion beam (FIB) (FEI Nova 600 NanoLab).

Electrochemical Measurements: Electrochemical measurements were carried out at 25 °C, using a VMP3 galvanostat potentiostat (Bio-Logic).

Solder-Reflow Thermal Treatments: Three successive thermal treatments, each reproducing a standardized temperature profile for lead-free reflow soldering,[29] were performed in industrial facilities with microbatteries (8.7 mm^2) embedded in an LGA package. The maximum temperature of 260 °C was maintained each time for about 30 s.

Supporting Information

Supporting Information is available from the Wiley Online Library or from the author.

Acknowledgements

This work was partly supported by the Agence Nationale de la Recherche during the project Mat&Pro EFiMi. Nicolas Dunoyer, Jean-Marc Boissel (CEA), and Laurent Figuière (ST Microelectronics) are acknowledged for the manufacture of microbatteries in the Endura cluster. The authors are also grateful to S. Sorieul from AIFIRA plateform (CENBG-CNRS/IN_2P_3-Bordeaux University) for her help in acquiring RBS spectra and M. Lahaye for Auger Electron Spectroscopy depth profiling.

Received: May 29, 2015
Revised: June 18, 2015
Published online: July 14, 2015

[1] B. Fleutot, B. Pecquenard, F. Le Cras, B. Delis, H. Martinez, L. Dupont, D. Guy-Bouyssou, *J. Power Sources* **2011**, *196*, 10289.
[2] T. Jimbo, P. Kim, K. Suu, *Energy Proc.* **2012**, *14*, 1574.
[3] B. Salam, C. Virseda, H. Da, N. N. Ekere, R. Durairaj, *Soldering Surf. Mount Technol.* **2004**, *16*, 27.
[4] B. J. Neudecker, N. J. Dudney, J. B. Bates, *J. Electrochem. Soc.* **2000**, *147*, 517.
[5] F. Sagane, K. Ikeda, K. Okita, H. Sano, H. Sakaebe, Y. Iriyama, *J. Power Sources* **2013**, *233*, 34.
[6] F. Sagane, R. Shimokawa, H. Sano, H. Sakaebe, Y. Iriyama, *J. Power Sources* **2013**, *225*, 245.
[7] B. J. Neudecker, R. A. Zuhr, J. B. Bates, *J. Power Sources* **1999**, *81*, 27.
[8] J. B. Bates, N. J. Dudney, B. Neudecker, A. Ueda, C. D. Evans, *Solid State Ionics* **2000**, *135*, 33.
[9] D. Li, Z. Ma, J. Xu, Y. Li, K. Xie, *Mater. Lett.* **2014**, *134*, 237.
[10] J. Lin, C. Liu, Q. Liu, H. Guo, *Appl. Mech. Mater.* **2014**, *496*, 38.
[11] J. Cabana, L. Monconduit, D. Larcher, M. R. Palacín, *Adv. Mater.* **2010**, *22*, E170.
[12] M. Baba, N. Kumagai, N. Fujita, K. Ohta, K. Nishidate, S. Komaba, H. Groult, D. Devilliers, B. Kaplan, *J. Power Sources* **2001**, *97*, 798.
[13] R. J. Zhu, Y. Ren, L. Q. Geng, T. Chen, L. X. Li, C. R. Yuan, *Mod. Phys. Lett. B* **2013**, *27*, 1350156.

[14] J. Schwenzel, V. Thangadurai, W. Weppner, *J. Power Sources* **2006**, *154*, 232.
[15] V. P. Phan, B. Pecquenard, F. Le Cras, *Adv. Funct. Mater.* **2012**, *22*, 2580.
[16] M. N. Obrovac, L. Christensen, *Electrochem. Solid-State Lett.* **2004**, *7*, A93.
[17] H. Y. Park, S. C. Nam, Y. C. Lim, K. G. Choi, K. C. Lee, G. B. Park, J. B. Kim, H. P. Kim, S. B. Cho, *Electrochim. Acta* **2007**, *52*, 2062.
[18] a) J. Li, A. K. Dozier, Y. Li, F. Yang, Y. T. Cheng, *J. Electrochem. Soc.* **2011**, *158*, A689; b) X. H. Liu, L. Zhong, S. Huang, S. X. Mao, T. Zhu, J. Y. Huang, *ACS Nano* **2012**, *6*, 1522.
[19] a) J. K. Yoo, J. Kim, Y. S. Jung, K. Kang, *Adv. Mater.* **2012**, *24*, 5452; b) J. Ji , H. Ji , L. L. Zhang, X. Zhao, X. Bai, X. Fan, F. Zhang, R. S. Ruoff, *Adv. Mater.* **2013**, *25*, 4673; c) X. Huang, J. Yang, S. Mao, J. Chang, P. B. Hallac, C. R. Fell, B. Metz, J. Jiang, P. T. Hurley, J. Chen, *Adv. Mater.* **2014**, *26*, 4326.
[20] M. Gu, Z. Wang, J. G. Connel, D. E. Perea, L. J. Lauhon, F. Gao, C. Wang, *ACS Nano* **2013**, *7*, 6303.
[21] S. Misra, N. Liu, J. Nelson, S. S. Hong, Y. Cui, M. F. Toney, *ACS Nano* **2012**, *6*, 5465.
[22] X. H. Liu, S. Huang, S. T. Picraux, J. Li, T. Zhu, J. Y. Huang, *Nano Lett.* **2011**, *11*, 3997.
[23] M. Ulldemolins, F. Le Cras, B. Pecquenard, *Electrochem. Commun.* **2013**, *27*, 22.
[24] V. Dubois, H. Martinez, A. Durand, B. Pecquenard, F. Le Cras, D. Guy-Bouyssou, (unpublished.).
[25] M. H. Lindic, B. Pecquenard, P. Vinatier, A. Levasseur, H. Martinez, D. Gonbeau, P. E. Petit, G. Ouvrard, *J. Electrochem. Soc.* **2005**, *152*, A141.
[26] J. Li , N. J. Dudney, X. Xiao, Y. T. Cheng, C. Liang, M. W. Verbrugge, *Adv. Energy Mater.* **2015**, *5*, 1401627.
[27] M. B. Dines, *Mater. Res. Bull.* **1975**, *10*, 287.
[28] M. Mayer, *SIMNRA User's Guide, Technical Report IPP 9/113*, Max Planck Institut für Plasmaphysik, Garching, Germany **1997**.
[29] Joint ICP/JEDEC standard J-STD-020D.1, Moisture/reflow sensitivity classification for nonhermetic solid.